Applied Surface Science 437 (2018) 390–399

Contents lists available at ScienceDirect

Applied Surface Science

journal homepage: www.elsevier.com/locate/apsusc

Full Length Article

Effect of Co addition on the performance and structure of V/ZrCe catalyst for simultaneous removal of NO and Hg^0 in simulated flue gas

Lingkui Zhao[a,b,c], Caiting Li[a,b,*], Xueyu Du[a,b], Guangming Zeng[a,b], Lei Gao[a,b], Yunbo Zhai[a,b], Teng Wang[a,b], Junyi Zhang[a,b]

[a] College of Environmental Science and Engineering, Hunan University, Changsha 410082, PR China
[b] Key Laboratory of Environmental Biology and Pollution Control (Hunan University), Ministry of Education, Changsha 410082, PR China
[c] College of Environmental Science and Resources, Xiangtan University, Xiangtan 411105, PR China

ARTICLE INFO

Article history:
Received 10 June 2017
Received in revised form 14 August 2017
Accepted 24 August 2017
Available online 1 September 2017

Keywords:
Vanadium
Cobalt oxide
Nitrogen oxide
NH_3–SCR
Hg^0 oxidation

ABSTRACT

The effect of CoO_x addition on the performance and structure of V_2O_5/ZrO_2–CeO_2 catalyst for simultaneous removal of NO and Hg^0 in simulated flue gas was investigated by various methods including SEM, BET, XRD, XPS, H_2–TPR and FT–IR. It was found that the introduction of CoO_x not only greatly enhanced the redox properties of catalysts, but also increased the catalytic performance for simultaneous removal of NO and Hg^0. The CoO_x–modified V_2O_5/ZrO_2–CeO_2 catalyst displayed excellent catalytic activity for NO conversion (89.6%) and Hg^0 oxidation (88.9%) at 250 °C under SCR atmosphere. The synergistic effect among vanadium, cobalt, and the ZrCe support could induce oxygen vacancies formation and promote oxygen mobility via charge transfer. Besides, CoO_x could assist vanadium species in rapidly changing the valence by the redox cycle of $V^{5+} + Co^{2+} \leftrightarrow V^{4+} + Co^{3+}$. All the above features contribute to the excellent catalytic performance through CoO_x addition.

1. Introduction

Coal–fired power plants are one of the biggest anthropogenic source of NO_x and mercury emissions because of high level of coal consumption. As major air pollutants, nitrogen oxides (NO_x) contribute to photochemical smog, acid rain, ozone depletion, and greenhouse effects [1]. Besides, mercury is one of the most hazardous environmental toxins and can be threat to both human health and the environment due to the extreme toxicity, persistence, and the bioaccumulation [2,3]. Therefore, how to control NO_x and mercury emissions from flue gas is becoming hotspot.

Up to now, various technologies and methods have been used to control NO_x and elemental mercury (Hg^0) emissions from coal plants, such as catalytic oxidation, activated carbon injection (ACI) capture, selective catalytic reduction (SCR), and photochemical oxidation [4–6]. Among available technologies, selective catalytic reduction of NO_x with NH_3 (NH_3–SCR) has been considered as one of the most promising technologies for simultaneous removal of NO and Hg^0, the core of which is to convert NO and Hg^0 to N_2 and Hg^{2+}, respectively [7–9]. The reasons are that integration of multiple treatment processes into a single unit could overcome the shortages of single–pollutant control technologies, including large occupying area, high operation cost and expensive equipment investment. Consequently, many novel and effective SCR catalysts have been studied for simultaneous removal of NO and Hg^0 [7–13]. However, according to our previous study [8], the V_2O_5/ZrO_2–CeO_2 catalysts are not effective enough for Hg^0 oxidation under SCR atmosphere, which may led to decreased interest in developing highly active and low-cost NH_3–SCR catalysts for simultaneous removal of NO and Hg^0. Therefore, it becomes more important to develop highly efficient NH_3–SCR catalysts for simultaneous removal of NO and Hg^0 under SCR atmosphere.

Recently, cobalt-based catalysts were widely used for NO removal and showed the promising activity for NO_x reduction [14–17]. At the same time, cobalt-based catalysts with excellent Hg^0 oxidation catalytic activity have also been attracting wide attention [18–20]. For example, Liu et al. [20] found that the CoO_x supported on titania was effective for Hg^0 oxidation within the temperature window of 120–330 °C. Zhang et al. [21] reported that the presence of CoO_x led to a better dispersion and more amorphous species of MnO_x over TiO_2, which would result in a better Hg^0 oxidation. Co–Ce mixed oxides supported on commercial cylindrical activated coke granulars showed excellent mercury removal ability [19]. Moreover, the high activity of CoO_x seemed to be resulted

* Corresponding author at: College of Environmental Science and Engineering, Hunan University, Changsha 410082, PR China.
E-mail addresses: ctli@hnu.edu.cn, ctli3@yahoo.com (C. Li).

https://doi.org/10.1016/j.apsusc.2017.08.165
0169-4332/

from the relatively low ΔH of vaporization of O_2 from lattice oxygen atom, which meant that the lattice oxygen was readily to be released at the relative low temperature range [22]. Typically, the combination of CeO_2 with other metal oxides often affects the oxygen mobility and the oxidation state of the element that is combined, which would effectively improve the elements' redox ability [23]. The literature reported that CoO_x/CeO_2 catalysts were very active for CO oxidation and their high activities were ascribed to finely dispersed and high valence state CoO_x which resulted from the synergistic interaction between cobalt oxides and ceria [24,25]. Previous researches also showed that the synergetic effect between V and Ce could result in the high catalytic performance [8,12,26,27]. Besides, Co and V are known to have variable valences, which is critical to the potential for intervalence charge transfer [28]. Inspired by these results, it was deduced that the combination of V, Co and Ce in one catalyst might facilitate the better catalytic performance for simultaneous removal of NO and Hg^0 due to the synergistic interaction among these three metal oxides. Unfortunately, the use of cobalt species to modify the performance and structure of $V_2O_5/ZrO_2–CeO_2$ catalyst for simultaneous removal of NO and Hg^0 has rarely been reported. In particular, the structure–activity relationship of the CoO_x–modified $V_2O_5/ZrO_2–CeO_2$ catalyst is still not very clear.

Accordingly, this work investigated the effect of cobalt oxide modification on the performance and structure of $V_2O_5/ZrO_2–CeO_2$ catalyst for simultaneous removal of NO and Hg^0 in simulated flue gas. A series of CoO_x–modified $V_2O_5/ZrO_2–CeO_2$ catalyst with various amounts of cobalt were synthesized and characterized by SEM, BET, XRD, XPS, H_2–TPR and FT–IR. Additionally, the synergistic effect among vanadium, cobalt, and the ZrCe support (V–Co–ZrCe) was also explored in light of the tests results and characterization techniques.

2. Experimental section

2.1. Catalyst synthesis

A series of CoO_x–modified $V_2O_5/ZrO_2–CeO_2$ were synthesized via impregnating the $ZrO_2–CeO_2$ (ZrCe) support (ZrCe support was prepared as our previously published reported [8]) with a mixture solution including the requisite amount of ammonium metavanadate and/or cobalt nitrate hexahydrate for 12 h. Subsequently, the impregnated materials were oven dried at 105 °C overnight and calcined at 500 °C for 3 h. Finally, all the samples were sieved with 100–120 mesh size. The obtained catalysts are labeled as $VCo_x/ZrCe$ ("x" refers the molar ratio of Co/(Zr + Ce); x = 0.05, 0.10, 0.15, 0.20, 0.25). The V_2O_5 content was set a relatively low level (the molar ratio of V/(Zr + Ce) was 0.01). The Co loading was described as the molar ratio of Co/(Ce + Zr). Typically, the molar ratio of Ce/Zr on all catalysts was 0.6.

2.2. Characterization

The surface morphology of the catalyst was analyzed by scanning electron microscopy (SEM) (Hitachi S–4800, Hitachi Limited, Japan). Brunauer–Emmett–Teller (BET) surface area and pore analysis were performed using a Micromeritics Tristar II 3020 analyzer (Micromeritics Instrument Crop, USA). X–ray diffraction (XRD) patterns were carried out on X-ray diffractometer (Rigaku rotaflex D/Max–C, Japan) with Cu–Ka radiation (λ = 1.5406 A°). X–ray Photoelectron Spectroscopy (XPS) analysis was taken on a K–Alpha 1063 system (Thermo Fisher Scientific, UK) with an Al Ka X–ray source. Fourier Transform Infrared Spectroscopy (FT–IR) was determined using a FTIR–8400S IRprestige–21 (SHIMADZU, Japan) apparatus. In order to remove any adsorbed species, the samples were pretreated at 250 °C in pure N_2 with a total flow rate of 500 mL/min for 30 min before each experiment. After that, NH_3 adsorption was conducted at room temperature for 60 min in a 700 ppm NH_3/N_2 flow (500 mL/min). Finally, the FT–IR experiments were carried out immediately. For NO + O_2 (700 ppm NO, 6% O_2/N_2), and $SO_2 + H_2O + O_2$ (300 ppm SO_2, 8 vol.%H_2O, 6% O_2/N_2) were collected at the similar procedure as the NH_3 adsorption. Temperature–programmed reduction of H_2 (H_2–TPR) measurements were carried out on an AutoChem 2920 automated chemisorption analyzer (Micromeritics Instrument Crop, USA). Prior to the experiments, the samples were pretreated by a pure N_2 flow at 300 °C for 30 min and then cooled to room temperature. Afterward, reduction performance was then recorded under 5 vol.% H_2 + 95 vol.%Ar stream (40 mL/min) from 50 to 750 °C at a heating rate of 10 °C/min.

2.3. Catalytic performance test

The activity tests for simultaneous removal of Hg^0 and NO were evaluated using a bench-scale experimental system, which was similar to that used in our previous study [8]. 0.25 g catalyst was placed into the fixed bed quartz reactor (i.d. 10 mm) with quartz wool. The simulated flue gas (SFG) consisted of 700 ppm NO, 700 ppm NH_3, 6% O_2, 300 ppm SO_2 (when used), and balance N_2. The Hg^0 permeation tube (VICI Metronics, USA) was used to generate 70.0 μg/m^3 Hg^0 vapor carried by pure N_2. The temperature of the teflon tubes that water vapor and Hg^0 passed through were kept at 120 °C to prevent water vapor and Hg^0 condensation. The total flow rate was 500 mL/min, and the corresponding gas hour space velocity (GHSV) was 100,000 h^{-1}. The reaction temperature was conducted from 100 to 400 °C. SCR atmosphere was defined as 700 ppm of NO, NH_3/NO = 1, 70.0 μg/m^3 Hg^0, and 6% O_2 balanced in N_2. After the catalytic reaction practically reached steady–state condition, the Hg^0 and NO concentrations in the inlet (Hg^0_{in}/NO_{in}) and outlet (Hg^0_{out}/NO_{out}) were analyzed by an online RA–915M mercury analyzer (LUMEX Ltd, Russia) and a flue gas analyzer (MGA5, Germany), respectively. According to previous studies [21,29,30], in order to avoid the possible bias because of Hg^0 physical adsorption, 0.25 g $VCo_x/ZrCe$ catalysts were saturated with 70.0 μg/m^3 Hg^0 under N_2 atmosphere at room temperature. Less than 10 min was needed for the adsorption experiment, suggesting that the Hg^0 physical adsorption capacity of $VCo_x/ZrCe$ catalysts was negligible. Accordingly, the NO conversion efficiency and Hg^0 oxidation efficiency was defined in Eqs. (1) and (2), respectively:

$$\eta_{NO}(\%) = \frac{NO_{in}\text{-}NO_{out}}{NO_{in}} \times 100\% \quad (1)$$

$$\eta_{Hg}(\%) = \frac{Hg^0_{in}\text{-}Hg^0_{out}}{Hg^0_{in}} \times 100\% \quad (2)$$

3. Results and discussion

3.1. Catalytic performance tests

3.1.1. Effect of CoOx addition on catalytic performance

The catalysts with different cobalt loadings were prepared to investigate the effect of CoO_x (Co) modification on the performance of $VCo_x/ZrCe$ catalyst. And the simultaneous removal performances of NO and Hg^0 over $VCo_x/ZrCe$ catalyst under different reaction temperature in SCR atmosphere are shown in Fig. 1. It was found that V/ZrCe catalyst exhibited the lowest activity. $VCo_{0.10}/ZrCe$ catalyst displayed excellent catalytic activity for NO conversion (89.6%) and Hg^0 oxidation (88.9%) at 250 °C under SCR atmosphere. Interestingly, when Co loading was lower than 0.10, catalytic activity for simultaneous removal of NO and Hg^0 gradually increased with increasing Co loading. However, further increase of Co load-

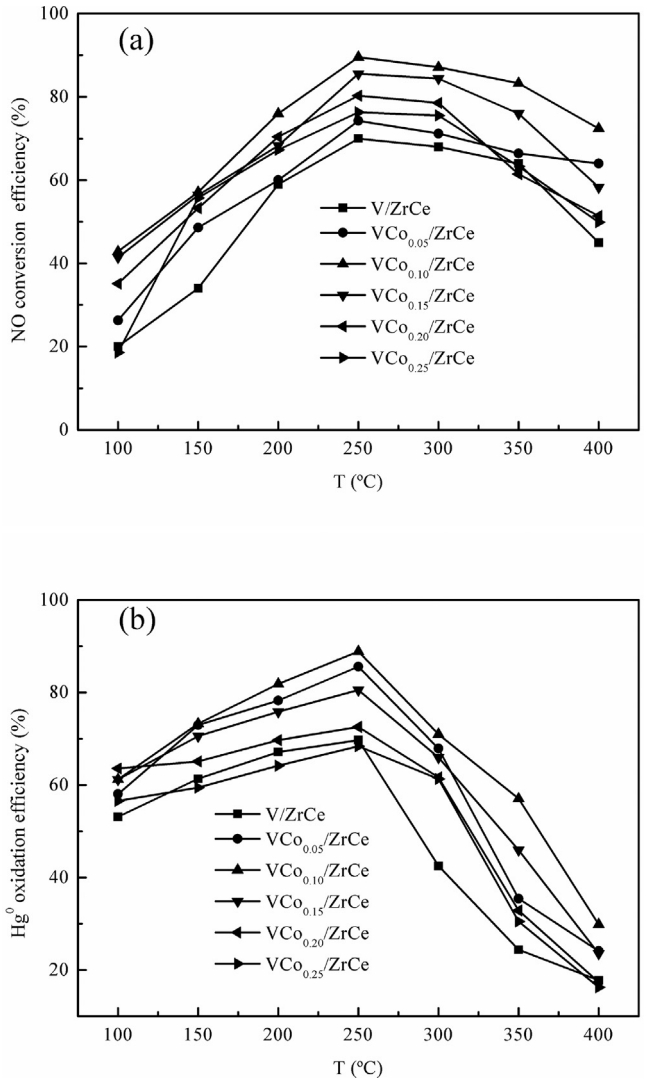

Fig. 1. Effect of CoO_x modification on simultaneous removal of NO and Hg^0 over $VCo_x/ZrCe$ catalysts in SCR atmosphere. (Reaction condition: 70.0 μg/m³ Hg^0, 700 ppm NO, NH_3/NO: 1, 6% O_2, 250 mg of sample, total flow rate 500 mL/min, GHSV 100,000 h^{-1}).

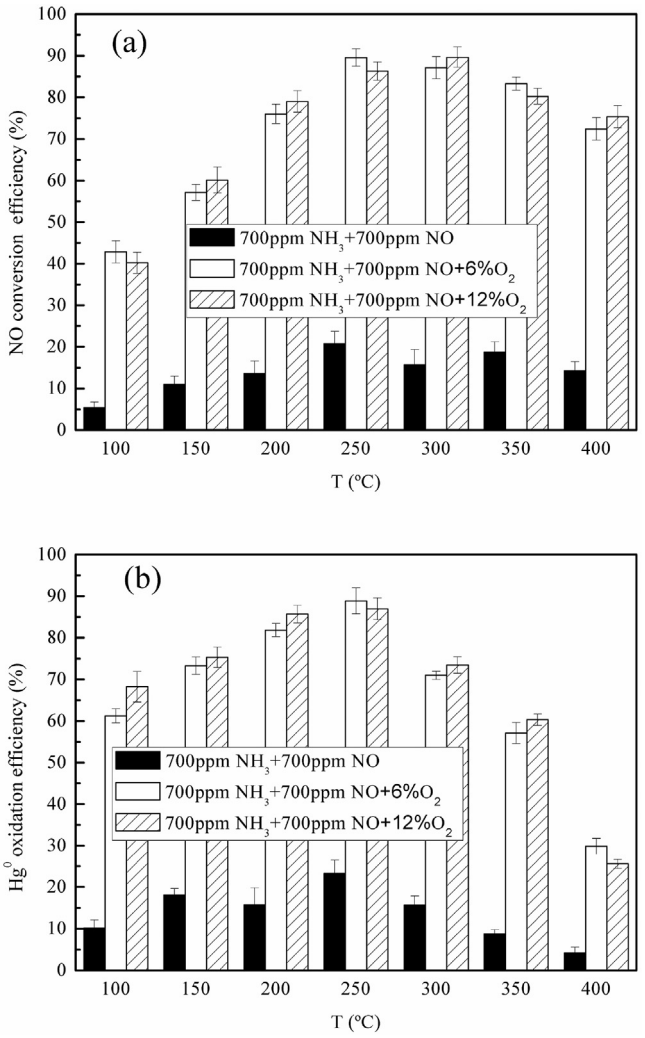

Fig. 2. Effect of O_2 concentration on simultaneous removal of NO and Hg^0 over $VCo_{0.10}/ZrCe$ catalysts. (Reaction condition: 70.0 μg/m³ Hg^0, 700 ppm NO, NH_3/NO: 1, 0–12% O_2, 250 mg of sample, total flow rate 500 mL/min, GHSV 100,000 h^{-1}).

ing resulted in the catalytic activity slightly decrease. The possible reason was that the active particle agglomeration over the external surface of samples caused blocking of the micropores, which was supported by SEM and BET results. Nevertheless, the catalytic activity over all $VCo_x/ZrCe$ was still higher than that of V/ZrCe. This suggested that Co modification could significantly improve the catalytic activities for simultaneous removal of NO and Hg^0. As evidenced by H_2–TPR and XPS, the reason for activity enhancement might be associated with the synergetic interaction among vanadium, cobalt, and the ZrCe support. On the one hand, the redox cycle ($V^{5+} + Co^{2+} \leftrightarrow V^{4+} + Co^{3+}$) could assist ZrCe support in supplying oxygen. On the other hand, CeO_2 could increase the number of reducing Co^{3+}, and then improve the reduction of Co^{3+} to Co^{2+} by facilitating the desorption of adsorbed oxygen species [31,32]. Furdermore, The SO_2 and H_2O tolerance of Co–modified V/ZrCe catalysts for simultaneous removal of NO and Hg^0 was studied as well. Results indicated that the catalysts showed remarkable SO_2 and H_2O resistance (Figs. S1 and S2).

3.1.2. *Effect of O_2*

The effect of O_2 concentration on simultaneous removal of Hg^0 and NO was investigated and the results are displayed in Fig. 2. It was clear that O_2 had significantly effect on the catalytic activity. There was almost negligible NO conversion (about 20.8%) and Hg^0 oxidation (about 23.3%) without O_2 (700 ppm NO, 700 ppm NH_3, 70.0 μg/m³ Hg^0) at 250 °C. Based on the results of H_2–TPR, XPS and FT-IR in this work, lattice oxygen may participate in NO conversion and Hg^0 oxidation. Although some previous studies have proposed that the presence of NH_3 had a serious adverse effect on Hg^0 oxidation due to the consumption of surface oxygen [3,8,27,33], the introduction of CoO_x could enhance oxygen mobility by improving the electron transfer on $VCo_{0.10}/ZrCe$ catalyst, which will be discussed later. That is, CoO_x–modified V_2O_5/ZrO_2–CeO_2 catalysts could easily capture gas–phase O_2 on the catalyst surface. The surface oxygen not only supplied abundant chemisorbed and lattice oxygen but also improved the formation of highly reactive surface nitrates [29,34]. Therefore, when 6%O_2 was added, there was a great increase of the catalytic activities for simultaneous removal of Hg^0 and NO. It also could explain why CoO_x–modified V_2O_5/ZrO_2–CeO_2 catalysts displayed excellent catalytic activity for NO conversion (89.6%) and Hg^0 oxidation (88.9%) under SCR atmosphere. However, when O_2 concentration further increased to 12%, no significant increase in catalytic activity was found, demonstrating that 6% O_2 was sufficient for NO conversion and Hg^0 oxidation.

3.2. Effect of CoOx addition on the structural properties of catalysts (SEM, BET, XRD)

3.2.1. SEM

The SEM experiments were undertaken to obtain more details about the effect of CoO_x modification on the structure of catalysts. As shown in Fig. 3, the microstructure of the V/ZrCe catalyst was greatly influenced by the introduction of CoO_x. For V/ZrCe catalyst, the surface was smooth and the size was uniform. However, a slight increase in the particle size was noticed after the addition of CoO_x, and the particle size increased with the increase of Co loading. For $VCo_{0.05}$/ZrCe and $VCo_{0.10}$/ZrCe catalyst with low Co loading, a few depositions formed, and the dispersion of activity species on the support surface was excellent, which was supported by XRD results. However, for $VCo_{0.15}$/ZrCe, $VCo_{0.20}$/ZrCe and $VCo_{0.25}$/ZrCe catalyst with high CoO_x loading, an apparent agglomeration of the activity species was observed. According to the literature [35], the strong interaction between the loading components and the ZrCe support could induce growth or aggregation of support crystallites during the calcination process. Therefore, the results could be inferred that the strong interaction may exist among vanadium, cobalt and the ZrCe support.

Table 1
The surface area, pore volume and pore diameter of the different catalysts.

Catalysts	BET surface area (m^2/g)	Pore volume (cm^3/g)	Average pore diameter (nm)
V/ZrCe	54.2	0.0642	4.74
$VCo_{0.05}$/ZrCe	58.2	0.0713	4.90
$VCo_{0.10}$/ZrCe	46.4	0.0518	4.47
$VCo_{0.15}$/ZrCe	38.9	0.0511	5.26
$VCo_{0.20}$/ZrCe	35.7	0.0485	5.44
$VCo_{0.25}$/ZrCe	36.4	0.0494	5.42

3.2.2. BET

The textural properties of catalysts are listed in Table 1. It could be found that $VCo_{0.05}$/ZrCe was of a highest surface area ($58.2\ m^2/g$) and pore volume ($0.0713\ cm^3/g$) among the samples. However, the surface area and pore volume decreased with the increasing of Co loading. Some researchers reported that the BET value is related to

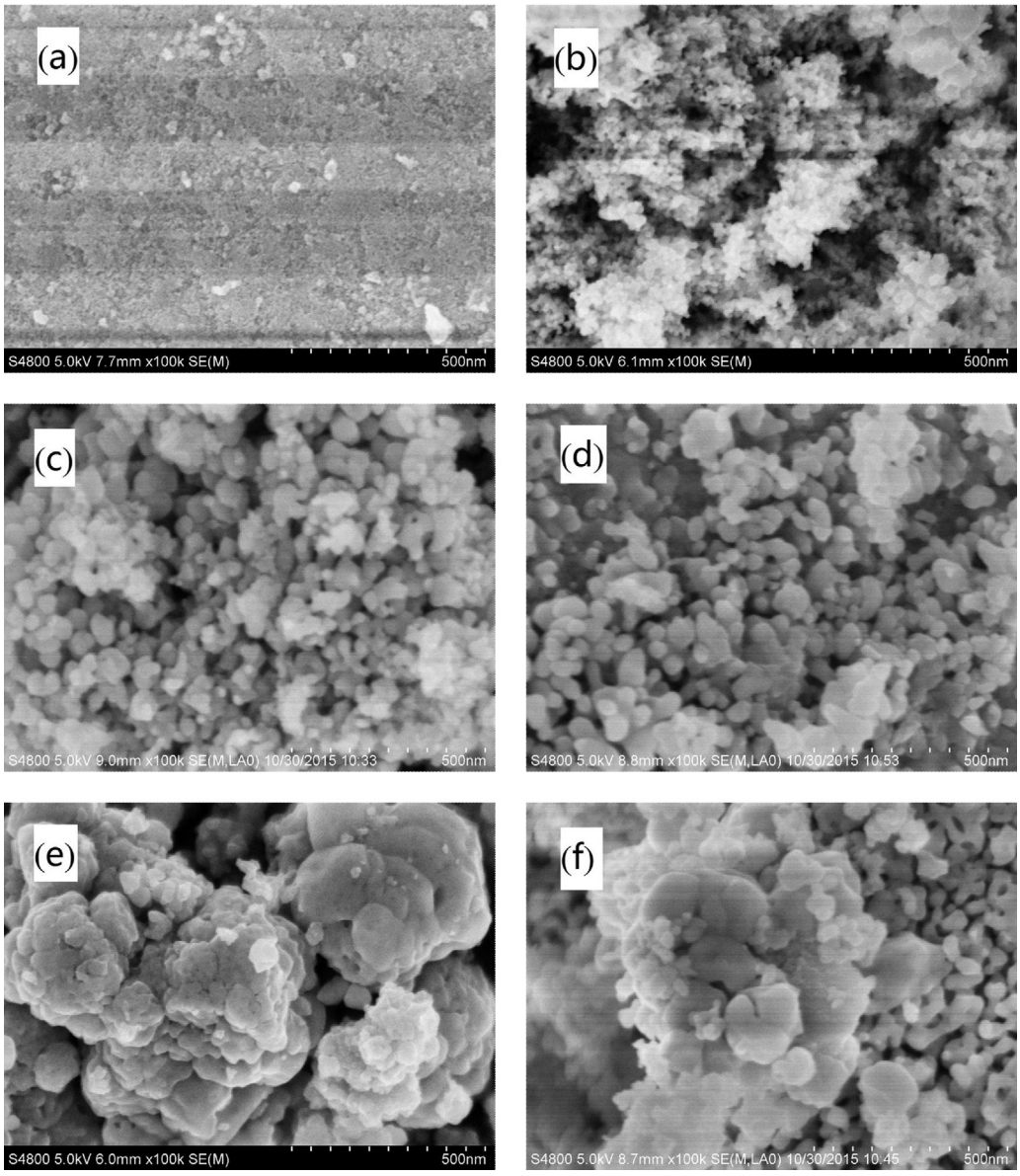

Fig. 3. SEM images of(a)V/ZrCe, (b)$VCO_{0.05}$/ZrCe, (c)$VCO_{0.10}$/ZrCe, (d)$VCO_{0.15}$/ZrCe, (e)$VCO_{0.20}$/ZrCe, (f)$VCO_{0.25}$/ZrCe.

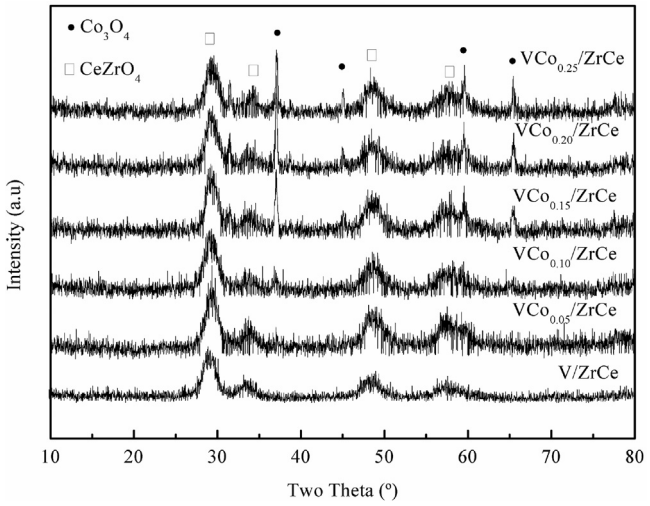

Fig. 4. XRD patterns of various catalysts.

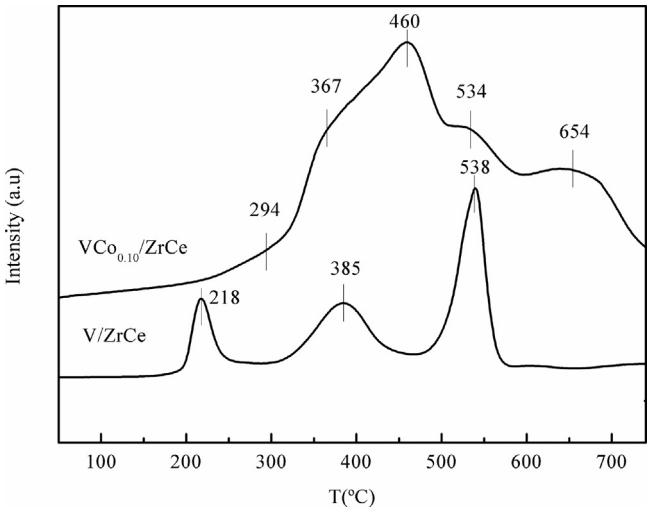

Fig. 5. H_2–TPR profiles of various catalysts.

the external surface area of the particles, which means that high surface area corresponds to small particle size and vice versa [36]. Combined with the SEM result, the particle size increased with the increasing of Co loading due to the strong interaction among vanadium, cobalt, and the ZrCe support. In addition, at higher Co loading, the aggregation of active components would block the micropores of carriers during the impregnation process and reduce the surface area as well (shown in Fig. 3).

3.2.3. XRD

The XRD technique was implemented to study the effect of CoO_x modification on the crystal structure of catalysts. As shown in Fig. 4, the XRD peaks for ZrCe almost did not shift after the introduction of CoO_x, indicating that the ZrCe support still maintained the cubic fluorite structure of $CeZrO_4$ (PDF–ICDD 54–0017) [37]. It was most likely that some vanadium and cobalt species might not incorporate into the bulk lattice of ZrCe binary oxide support to form a new solid solution. Besides, for those samples, the characteristic diffraction peaks of crystalline vanadium oxide did not appear, which was probably due to well dispersion or amorphous structure on the ZrCe support. It was worth noting that no diffraction peaks for crystalline Co_3O_4 (PDF–ICDD 09–0418) [38] were detected when Co loading was less than 0.10, suggesting that cobalt oxide species show well dispersion. However, with further increasing the Co loading, the characteristic peaks of crystalline Co_3O_4 were observed. It might be because that cobalt oxide species were aggregated, which was also supported by SEM results.

3.3. Effect of CoO_x addition on the redox properties (H_2–TPR)

As illustrated in Fig. 5, H_2–TPR techniques were conducted to study the effect of Co modification on the redox properties of catalysts. Some researchers have reported that no any reduction peak shown below 900 °C over pure ZrO_2 [37,39]. Therefore, the TPR peaks for V/ZrCe catalyst at this temperature region could be mainly assigned to the reduction of vanadium and cerium species. It could be seen that the TPR profile of V/ZrCe showed three obvious reduction peaks at around 218, 385 and 538 °C. Due to the increasing polymerization degree of VO_x species, the first peak at 218 °C was assigned to the facile reduction of VO_x species, and the peak at 385 °C could be attributed to the reduction of polymeric VO_x species formed by connecting isolated VO_x species with bridging oxygen [40]. The peak at 538 °C would be ascribed to the reduction of Ce^{4+} to Ce^{3+} [41]. For $VCo_{0.10}$/ZrCe catalyst, five peaks appeared at approximately 294, 376, 460, 534 and 654 °C. According to the literatures [42–44], the shoulder peak at 294 °C and 376 °C should be the stepwise reduction of cobalt oxide species, which could be corresponded to the reduction of Co^{3+} ions to Co^{2+} and Co^{2+} to metallic cobalt, respectively. The peak at 460 °C was ascribed to reduction of V^{5+} to V^{4+} [26,45]. The peak at 534 °C was caused by the reduction of Ce^{4+} to Ce^{3+} [41]. The peak at 654 °C could be attributed to the reduction of lattice oxygen [46]. These results demonstrated that the addition of CoO_x greatly enhance the redox ability of catalyst. Combined with the results of XPS, it could be inferred that synergistic effect existed among vanadium, cobalt, and ZrCe support. Higher the redox properties of $VCo_{0.10}$/ZrCe catalyst could promoted the mobility of surface oxygen because of the strong synergetic effect among vanadium, cobalt, and ZrCe support.

3.4. Surface oxidation state of catalysts (XPS)

The XPS spectra of Co 2p, V 2p, Ce 3d, O 1s and Hg 4f are shown in Fig. 6. The used $VCo_{0.10}$/ZrCe catalyst had been tested under SCR atmosphere at 250 °C. Some researchers have reported that the Co 2p region consisted of a spin–orbit doublet with Co 2p1/2 and Co 2p3/2 [21,47]. As depicted in Fig. 6(a), the binding energy of 780.4 eV was assigned to Co 2p3/2, which was characteristic of a mixed–valence cobalt system (Co^{3+} and Co^{2+}) [31]. As the 2p3/2 binding energies of Co^{2+} are relatively close to that of Co^{3+}, the two oxidation states of cobalt could be distinguished by a distinct shake up satellite at about 786.4 eV [24]. It was found that two peaks at 780.2 and 782.3 eV were assigned to Co^{3+} and Co^{2+} species, respectively [32]. According to the peak areas, the oxidation states of Co^{3+} were the primary form. After the reaction, the main peak of Co 2p3/2 state shifted to lower binding energy, implying that the interaction between cobalt species and vanadium species/support led to chemical shift. More significantly, the Co^{2+}/Co^{3+} ratio increased from 0.4 to 1.8 after the reaction, demonstrating that some Co^{3+} was reduced to Co^{2+} during the reaction. Concerning the V 2p spectra (seen in Fig. 6(b)), it was apparent that the chemical valence of vanadium on the surface of V/ZrCe catalyst was mainly in a 4+ oxidation state, and a small quantity of a 5+ co–existed. After the introduction of cobalt oxide, V^{5+} oxidation states increased. Interestingly, the V^{4+}/V^{5+} ratio of $VCo_{0.10}$/ZrCe catalyst increased from 0.9 to 1.6 after the reaction, suggesting that the reduction of V^{5+} to V^{4+} was occurred. The generation of V^{4+} together with observation of Co^{2+} species was demonstrative of synergetic effect between vanadium and cobalt via charge transfer (i.e., $V^{5+} + Co^{2+} \leftrightarrow V^{4+} + Co^{3+}$), which further confirmed the earlier deduction from H_2–TPR. CoO_x

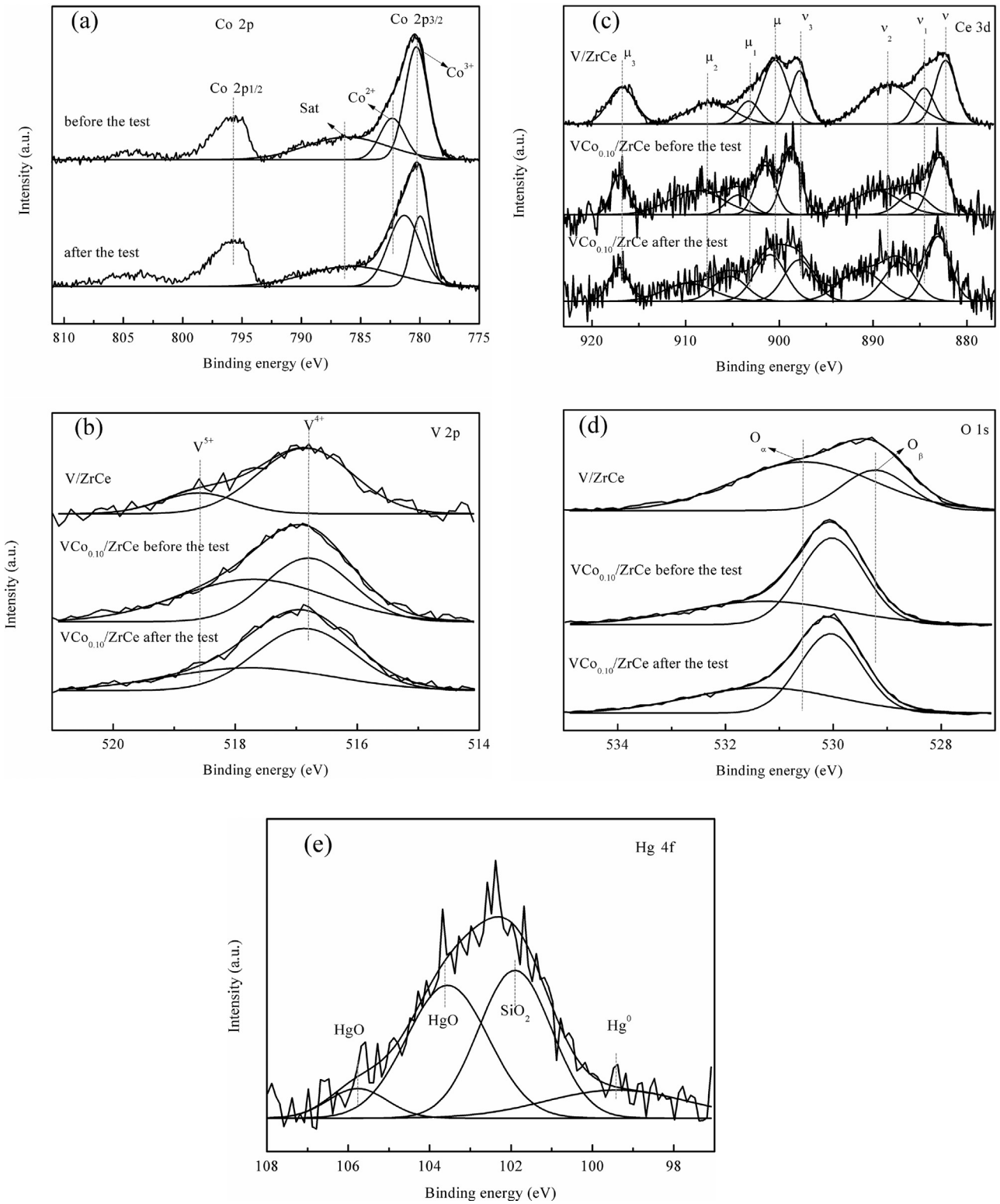

Fig. 6. XPS spectra of V/ZrCe and $VCo_{0.10}$/ZrCe catalysts over the spectral regions of Co 2p, V 2p, Ce 3d and O 1s before the test; and Co 2p, V 2p, Ce 3d, O 1s, and Hg 4f after the test (Reaction condition: 70.0 μg/m^3 Hg^0, 700 ppm NO, NH_3/NO: 1, 6% O_2, 250 mg of sample, 500 mL/min total flow rate and GHSV 100,000 h^{-1}).

could assist vanadium species in rapidly changing the valence by the redox cycle of $V^{5+} + Co^{2+} \leftrightarrow V^{4+} + Co^{3+}$.

As shown in Fig. 6(c), the Ce 3d spectrum can be resolved into eight components. The bands labeled u, u_2, u_3, v, v_2 and v_3 were ascribed to Ce^{4+}, while the peaks labeled u_1 and v_1 were corresponded to Ce^{3+} oxides [48,49]. It could be seen that Ce^{4+} and Ce^{3+} co–existed in the surface of V/ZrCe catalysts, and the valence of cerium was predominant in a 4+. When CoO_x was added into the catalysts, the Ce 3d peaks slightly shifted to higher binding energy. Besides, the Ce^{3+}/Ce^{4+} ratio increased from 0.1 to 0.2. This revealed that the Ce^{3+}/Ce^{4+} ratio on the sample was enhanced by the introduction of cobalt oxide. In general, the presence of Ce^{3+}

favors the formation of oxygen vacancies (Vo) and promotes the adsorption and activation of oxygen species [50,51]. The oxygen vacancies has been proposed to occur by the following equation: $Vo + O_2 + e^- \rightarrow$ adsorbed oxygen [52]. After the reaction, the intensity of u_1 and v_1 for Ce^{3+} increased, and the ratio of Ce^{3+}/Ce^{4+} further increased to 0.3. It has been reported that oxygen species could be stored/released by ceria via the redox shift between Ce^{3+}/Ce^{4+}, leading to the increase of surface mobile oxygen [8,53]. Taken together, these observations can be speculated that a synergistic effect exists among vanadium, cobalt, and the ZrCe support, which could induce oxygen vacancies formation and enhance oxygen mobility.

Fig. 6(d) shows O 1s XPS spectra of the V/ZrCe, fresh $VCo_{0.10}$/ZrCe and the used $VCo_{0.10}$/ZrCe catalyst. For V/ZrCe catalyst, the peak at around 529.2 eV was indicative of the lattice oxygen (denoted as (O_β)), whereas the peak at around 530.5 eV was corresponded to the chemisorbed oxygen (denoted as (O_α)) [54,55]. Remarkably, the introduction of CoO_x led to the chemical shift of O_α and O_β signals to higher binding energy. It was evident that binding energy of O_β and O_α moved from 529.2 to 530.0 eV and from 530.5 to 531.3 eV, respectively. This may be due to the electronic state interaction of V–Co–ZrCe, which might facilitate the reducibility of active species and the formation of oxygen vacancies. Moreover, the ratio of O_β, calculated by $O_\beta/(O_\alpha + O_\beta)$, over fresh $VCo_{0.10}$/ZrCe (60.8%) was higher than that over V/ZrCe (28.5%), demonstrating that the introduction of Co to V/ZrCe favorably supplied O_β rather than O_α. It was noteworthy that the ratio of O_β on the $VCo_{0.10}$/ZrCe catalyst decreased from 60.8% to 56.7% after the reaction, suggesting that the adsorbed Hg^0 was mainly oxidized by the lattice oxygen species. At the same time, the ratio of $O_\alpha/(O_\alpha + O_\beta)$ increased from 39.2% to 43.3%. This should be because of the presence of Ce^{3+} over the $VCo_{0.10}$/ZrCe catalyst that favored the formation of oxygen vacancy in the oxide surface. Additionally, it was hypothesized that the synergistic effects among vanadium, cobalt and ZrCe support might lead to the active oxygen migration from ZrCe support to vanadium and cobalt sites. Therefore, combined with all above results, the addition of cobalt oxide could enhance the redox of catalyst due to the redox equilibrium $V^{5+} + Co^{2+} \leftrightarrow V^{4+} + Co^{3+}$ and assist ZrCe support in supplying oxygen because of the interaction of V–Co–ZrCe, thereby synergistically enhancing the activity for NO conversion and Hg^0 oxidation.

Fig. 6(e) depicts the Hg 4f XPS patterns. The peak at 99.4 eV was attributed to Hg^0 [56]. Two characteristic peaks at 101.9 and 105.8 eV for Hg 4f can be ascribed to HgO [57,58]. The peak at 103.5 eV was corresponded to Si 2p of SiO_2 in quartz wool [59,60]. It illustrated that the majority of mercury species existed as HgO on the surface of $VCo_{0.10}$/ZrCe. Combining the results of this work and the previous studies [8,61,62], a likely reaction of Hg^0 oxidation followed the Mars–Maessen mechanism.

3.5. FT–IR study

FT–IR characterization of $VCo_{0.10}$/ZrCe catalyst at different gas compositions for 60 min was used in this section to further investigate the NH_3 and NO_x adsorption abilities. Fig. 7 displays the FT–IR spectra results of NH_3 and $NO + O_2$ adsorption over $VCo_{0.10}$/ZrCe catalyst. As shown in Fig. 7(a), the sample under different gas compositions showed two distinct bands that were due to the Co—O stretching vibration of cobaltic oxide. The first band at 567 cm^{-1} was the characteristic vibration of Co^{3+} in octahedral holes and the second band at 661 cm^{-1} was attributed to the vibration of Co^{2+} in tetrahedral holes [42,63,64]. This result further demonstrated that some Co^{3+} was reduced to Co^{2+} during the reaction, which was further confirmed the results of H_2–TPR and XPS.

As shown in Fig. 7(b), after adsorption of NH_3, the catalyst exhibited the largest amount of NH_3 linked to Lewis acid sites and NH_4^+ bound to Bronsted acid sites, which was beneficial for NO conversion. It could be seen that the bands at 1630 cm^{-1} and 1216 cm^{-1}, 1099 cm^{-1} were ascribed to asymmetric and symmetric bending vibrations of N—H bonds in coordinated NH_3 linked to Lewis acid sites, respectively [65,66]. Furthermore, the bands at 1425 cm^{-1} and 1340 cm^{-1} attributed to asymmetric and symmetric bending vibrations of NH_4^+ species on Brønsted acid sites were also detected [66–68]. The weak bands in the range of 1511–1556 cm^{-1} were conjectured as the intermediate products of NH_3–SCR reaction such as amide species (—NH_2), indicating partial oxidation (or dehydrogenation) of the adsorbed NH_3 would took place over the catalyst [69,70].

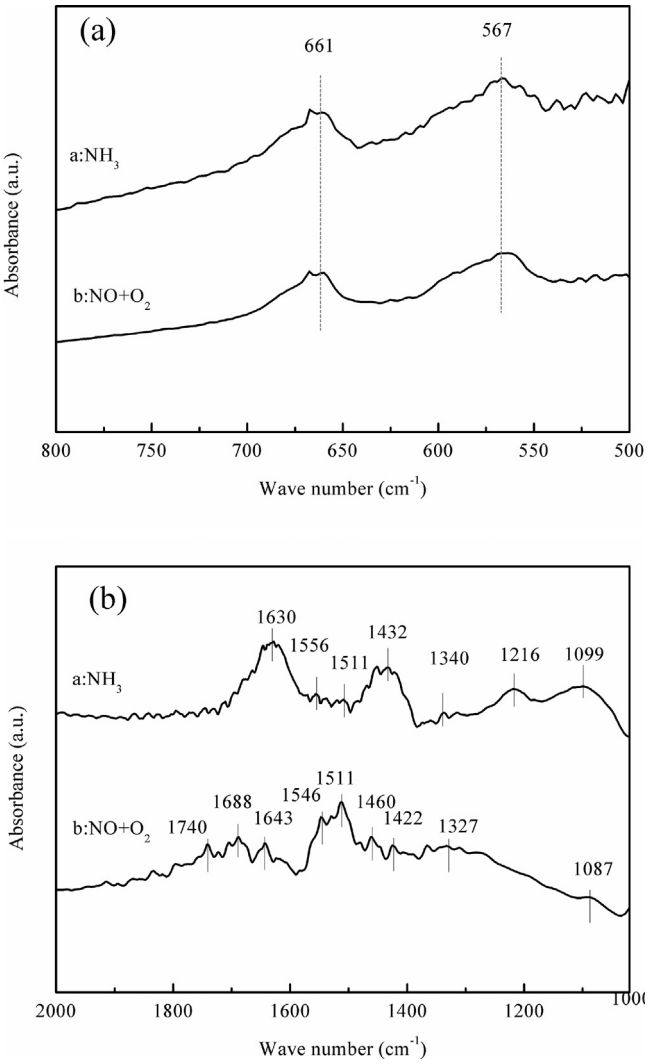

Fig. 7. FT-IR spectra taken upon $VCo_{0.10}$/ZrCe catalysts.

In ($NO + O_2$) FT–IR curve, several bands at 1740, 1688, 1643, 1546, 1511, 1460, 1422, 1327 and 1087 cm^{-1} were observed. The bands at 1688 and 1643 cm^{-1} were attributed to bridging nitrate [71]. The broad peak in the range of 1546–1511 cm^{-1} could be corresponded to NO_2–containing species, like nitrito (O—bound NO_2) and nitrato (NO_3) species [66]. Three bands at 1327 cm^{-1} (M—NO_2 nitro compounds) [72], 1460 cm^{-1} (monodentate nitrates) [73] and 1422 cm^{-1} (monodentate nitrates) [73] could be assigned to the reaction of produced NO_2 with surface oxygen [34]. The band at 1087 cm^{-1} was corresponded to anionic nitrosyl NO— species [74]. The discussion of FT–IR above showed that the adsorbed N species existed mainly as nitrates species which could take part in redox reaction sufficiently [34,75].

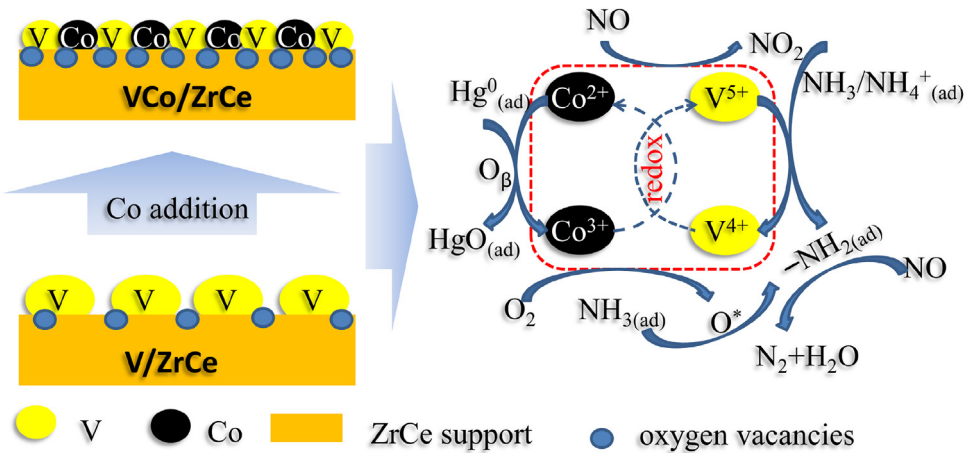

Fig. 8. Mechanism of CoO_x-modified V_2O_5/ZrO_2-CeO_2 catalyst for simultaneous removal of NO and Hg^0.

3.6. Mechanism for simultaneous removal of NO and Hg^0 over $VCo_{0.10}/ZrCe$

On the basis of literatures [8,34,69,76,77] and the results above, a possible mechanism for simultaneous removal of NO and Hg^0 over CoO_x–modified V_2O_5/ZrO_2–CeO_2 catalyst is showed in Fig. 8. On the one hand, Co^{3+}/Co^{2+} redox could improve V^{5+}/V^{4+} redox via the redox equilibrium of $V^{5+} + Co^{2+} \leftrightarrow V^{4+} + Co^{3+}$, which was beneficial to the simultaneous removal of NO and Hg^0. On the other hand, the strong interaction among vanadium, cobalt, and the ZrCe support was also greatly contributed to the higher activity. When some vanadium and cobalt species incorporated into the surface/subsurface lattice of the ZrCe support, it made cubic fluorite structure of $CeZrO_4$ more defective, hence forming oxygen vacancies with high mobility at catalysts surface.

For Hg^0 oxidation, our present works suggested that the process of Hg^0 oxidation over CoO_x–modified V_2O_5/ZrO_2–CeO_2 catalysts followed the Mars–Maessen mechanism. In this process, gas-phase Hg^0 ($Hg^0_{(g)}$) was firstly adsorbed over catalysts surface to generate $Hg^0_{(ad)}$, then V_2O_5 and CoO_x offer the lattice oxygen for $Hg^0_{(ad)}$ oxidation. The reduced V_2O_5 and CoO_x was re-oxidized by $O_{2(g)}$ in flue gas. The redox equilibrium of $V^{5+} + Co^{2+} \leftrightarrow V^{4+} + Co^{3+}$ promoted the reducibility of vanadium species, and ZrCe support could easily captured the $O_{2\,(g)}$ to refresh the reduced V_2O_5 and CoO_x because of abundant oxygen vacancies on its surface. Based on the discussion above, the mechanism for Hg^0 oxidation could be described as follows:

$$Hg^0(g) \rightarrow Hg^0(ad) \quad (3)$$

$$Hg^0(ad) + O_\beta \rightarrow HgO_{(ad)} \quad (4)$$

$$V_2O_5 \rightarrow V_2O_4 + O_\beta \quad (5)$$

$$Co_3O_4 \rightarrow 3CoO + O_\beta \quad (6)$$

$$V_2O_4 + \frac{1}{2}O_{2(g)} \rightarrow V_2O_5 \quad (7)$$

$$3CoO + \frac{1}{2}O_2 \rightarrow Co_3O_4 \quad (8)$$

$$V_2O_5 + 3CoO \leftrightarrow V_2O_4 + Co_3O_4 \quad (9)$$

For NO conversion, the possible SCR reaction on the catalysts could be illustrated as follows:

$$O_2(g) \rightarrow O^*(ad) \quad (10)$$

$$NH_3(g) \rightarrow NH_3(ad) \quad (11)$$

$$NH_3(g) \rightarrow NH_4^+(ad) \quad (12)$$

$$2NO(g) + O_2(g) \rightarrow 2NO_2(ad) \quad (13)$$

$$2NH_3(ad) + NO_2(ad) + NO(g) \rightarrow 2N_2 + 3H_2O \quad (14)$$

$$2NH_4^+(ad) + NO_2(ad) + NO(g) \rightarrow 2N_2 + 3H_2O + 2H^+ \quad (15)$$

$$NH_3(ad) + O^*(ad) \rightarrow NH_4(ad) + OH(ad) \quad (16)$$

$$NO(ad) + NH_2(ad) \rightarrow NH_2NO(ad) \rightarrow N_2(g) + H_2O(g) \quad (17)$$

Initially, gaseous NH_3 was adsorbed onto Lewis and Brønsted acid sites over the catalyst surface to generate coordinated NH_3, NH_4^+, and other intermediates from NH_3 oxidation. At the same time, NO could be oxidized by labile oxygen to form NO_2–containing species in the presence of O_2. According to the literature [34,78], the lattice oxygen on the surface of catalyst acted as a "transfer station" in the NH_3–SCR, especially in the oxidation of NH_3, while the main function of the gaseous oxygen in the flue gas was filling the vacancies on the surface of catalyst. In this work, the labile oxygen/lattice oxygen was released from the valence state change of V_2O_5 and CoO_x. The ZrCe support acted as the oxygen storage promoter. Then the adsorbed NH_3 or NH_4^+ species could react with gaseous NO to form the key intermediate species (NH_2NO), which finally decomposed into N_2 and H_2O. In addition, $-NH_2$ could react with NO to form intermediate species (NH_2NO) as well. Afterward, the gaseous O_2 in the flue gas was filled the vacancies of ZrCe support again before the beginning of next reduction–oxidation cycle.

4. Conclusions

The major aim was to investigate the effect of CoO_x modification on the performance and structure of V_2O_5/ZrO_2–CeO_2 catalyst for simultaneous removal of NO and Hg^0 in simulated flue gas. A series of CoO_x–modified V_2O_5/ZrO_2–CeO_2 catalysts were synthesized and characterized by SEM, BET, XRD, XPS, H_2–TPR and FT–IR. Results suggested that CoO_x–modified V_2O_5/ZrO_2–CeO_2 catalyst exhibited superior NO conversion (89.6%) and Hg^0 oxidation (88.9%) at 250 °C under SCR atmosphere. The addition of cobalt species not only enhanced the redox properties of catalysts, but also promoted the catalytic performance for simultaneous removal of NO and Hg^0. The valence of vanadium species could rapidly change via the redox cycle of $V^{5+} + Co^{2+} \leftrightarrow V^{4+} + Co^{3+}$. In particular, the introduction of cobalt species could induce oxygen vacancies formation and improve the oxygen mobility due to the strong interaction among vanadium, cobalt, and the ZrCe support. These factors were favorable for the remarkable catalytic performance through CoO_x addition.

Acknowledgments

This project was financially supported by the National Natural Science Foundation of China (51478173), the National Key Research and Development Program of China (2016YFC0204104) and the Scientific and Technological Major Special Project of Hunan Province in China (2015SK1003)

Appendix A. Supplementary data

Supplementary data associated with this article can be found, in the online version, at http://dx.doi.org/10.1016/j.apsusc.2017.08.165.

References

[1] W. Chen, Y. Ma, Z. Qu, Q. Liu, W. Huang, X. Hu, N. Yan, Mechanism of the selective catalytic oxidation of slip ammonia over Ru-modified Ce–Zr complexes determined by in situ diffuse reflectance infrared Fourier transform spectroscopy, Environ. Sci. Technol. 48 (2014) 12199–12205.
[2] W. Chen, Y. Pei, W. Huang, Z. Qu, X. Hu, N. Yan, Novel effective catalyst for elemental mercury removal from coal-fired flue gas and the mechanism investigation, Environ. Sci. Technol. 50 (2016) 2564–2572.
[3] H. Xu, Z. Qu, C. Zong, F. Quan, J. Mei, N. Yan, Catalytic oxidation and adsorption of Hg^0 over low-temperature NH_3-SCR $LaMnO_3$ perovskite oxide from flue gas, Appl. Catal. B 186 (2016) 30–40.
[4] Y. Gao, Z. Zhang, J. Wu, L. Duan, A. Umar, L. Sun, Z. Guo, Q. Wang, A critical review on the heterogeneous catalytic oxidation of elemental mercury in flue gases, Environ. Sci. Technol. 47 (2013) 10813–10823.
[5] Y. Liu, Y.G. Adewuyi, A review on removal of elemental mercury from flue gas using advanced oxidation process: chemistry and process, Chem. Eng. Res. Des. 112 (2016) 199–250.
[6] Y. Liu, Q. Wang, Removal of elemental mercury from flue gas by thermally activated ammonium persulfate in a bubble column reactor, Environ. Sci. Technol. 48 (2014) 12181–12189.
[7] L. Zhao, C. Li, Y. Wang, H. Wu, L. Gao, J. Zhang, G. Zeng, Simultaneous removal of elemental mercury and NO from simulated flue gas using a CeO_2 modified V_2O_5-WO_3/TiO_2 catalyst, Catal. Sci. Technol. 6 (2016) 6076–6086.
[8] L. Zhao, C. Li, S. Li, Y. Wang, J. Zhang, T. Wang, G. Zeng, Simultaneous removal of elemental mercury and NO in simulated flue gas over V_2O_5/ZrO_2-CeO_2 catalyst, Appl. Catal. B 198 (2016) 420–430.
[9] Y. Wang, B. Shen, C. He, S. Yue, F. Wang, Simultaneous removal of NO and Hg-0 from flue gas over Mn-Ce/Ti-PILCs, Environ. Sci. Technol. 49 (2015) 9355–9363.
[10] J. He, G.K. Reddy, S.W. Thiel, P.G. Smirniotis, N.G. Pinto, Simultaneous removal of elemental mercury and NO from flue gas using CeO_2 modified MnO_x/TiO_2 materials, Energy Fuel 27 (2013) 4832–4839.
[11] H. Chang, Q. Wu, T. Zhang, M. Li, X. Sun, J. Li, L. Duan, J. Hao, Design strategies for CeO_2–MoO_3 catalysts for DeNOx and hg0 oxidation in the presence of HCl: the significance of the surface acid–base properties, Environ. Sci. Technol. 49 (2015) 12388–12394.
[12] X. Zhang, C. Li, L. Zhao, J. Zhang, G. Zeng, Simultaneous removal of elemental mercury and NO from flue gas by V_2O_5–CeO_2/TiO_2 catalysts, Appl. Surf. Sci. 347 (2015) 392–400.
[13] T. Wang, C. Li, L. Zhao, J. Zhang, S. Li, G. Zeng, The catalytic performance and characterization of ZrO2 support modification on CuO-CeO_2/TiO_2 catalyst for the simultaneous removal of Hg^0 and NO, Appl. Surf. Sci. 400 (2017) 227–237.
[14] M.F. Irfan, J.H. Goo, S.D. Kim, Co_3O_4 based catalysts for NO oxidation and NO x reduction in fast SCR process, Appl. Catal. B 78 (2008) 267–274.
[15] L.B. Gutierrez, E.E. Miró, M.A. Ulla, Effect of the location of cobalt species on NO adsorption and NO_x-SCR over Co–mordenite, Appl. Catal. A 321 (2007) 7–16.
[16] C. He, M. Paulus, W. Chu, J. Find, J.A. Nickl, K. Köhler, Selective catalytic reduction of NO by C_3H_8 over CoO_x/Al_2O_3: an investigation of structure–activity relationships, Catal. Today 131 (2008) 305–313.
[17] B. Thirupathi, P.G. Smirniotis, Co-doping a metal (Cr, Fe, Co, Ni, Cu, Zn, Ce, and Zr) on Mn/TiO_2 catalyst and its effect on the selective reduction of NO with NH3 at low-temperatures, Appl. Catal. B 110 (2011) 195–206.
[18] J. Yang, Y. Zhao, L. Chang, J. Zhang, C. Zheng, Mercury adsorption and oxidation over cobalt oxide loaded magnetospheres catalyst from fly ash in oxyfuel combustion flue gas, Environ. Sci. Technol. 49 (2015) 8210–8218.
[19] H. Wu, C. Li, L. Zhao, J. Zhang, G. Zeng, Y. e. Xie, X. Zhang, Y. Wang, Removal of gaseous elemental mercury by cylindrical activated coke loaded with CoO_x-CeO_2 from simulated coal combustion flue gas, Energy Fuel 29 (2015) 6747–6757.
[20] Y. Liu, Y. Wang, H. Wang, Z. Wu, Catalytic oxidation of gas-phase mercury over Co/TiO_2 catalysts prepared by sol–gel method, Catal. Commun. 12 (2011) 1291–1294.
[21] A. Zhang, W. Zheng, J. Song, S. Hu, Z. Liu, J. Xiang, Cobalt manganese oxides modified titania catalysts for oxidation of elemental mercury at low flue gas temperature, Chem. Eng. J. 236 (2014) 29–38.
[22] L. Liu, Y. Chen, L. Dong, J. Zhu, H. Wan, B. Liu, B. Zhao, H. Zhu, K. Sun, L. Dong, Investigation of the NO removal by CO on CuO–CoOx binary metal oxides supported on $Ce_{0.67}Zr_{0.33}O_2$, Appl. Catal. B 90 (2009) 105–114.
[23] S. Imamura, M. Shono, N. Okamoto, A. Hamada, S. Ishida, Effect of cerium on the mobility of oxygen on manganese oxides, Appl. Catal. A 142 (1996) 279–288.
[24] M. Kang, M.W. Song, C.H. Lee, Catalytic carbon monoxide oxidation over CoO x/CeO_2 composite catalysts, Appl. Catal. A 251 (2003) 143–156.
[25] Q. Guo, Y. Liu, MnOx modified Co_3O_4-CeO_2 catalysts for the preferential oxidation of CO in H_2-rich gases, Appl. Catal. B 82 (2008) 19–26.
[26] Z. Liu, S. Zhang, J. Li, J. Zhu, L. Ma, Novel V_2O_5–CeO_2/TiO_2 catalyst with low vanadium loading for the selective catalytic reduction of NOx by NH3, Appl. Catal. B 158–159 (2014) 11–19.
[27] L. Zhao, C. Li, J. Zhang, X. Zhang, F. Zhan, J. Ma, Y. e. Xie, G. Zeng, Promotional effect of CeO_2 modified support on V_2O_5–WO_3/TiO_2 catalyst for elemental mercury oxidation in simulated coal-fired flue gas, Fuel 153 (2015) 361–369.
[28] W.F. Chen, P. Koshy, C.C. Sorrell, Effect of intervalence charge transfer on photocatalytic performance of cobalt- and vanadium-codoped TiO_2 thin films, Int. J. Hydrogen Energy 40 (2015) 16215–16229.
[29] H. Li, C.Y. Wu, Y. Li, J. Zhang, Superior activity of MnO_x-CeO_2/TiO_2 catalyst for catalytic oxidation of elemental mercury at low flue gas temperatures, Appl. Catal. B 111–112 (2012) 381–388.
[30] H. Li, C.Y. Wu, Y. Li, J.Y. Zhang, CeO_2-TiO_2 catalysts for catalytic oxidation of elemental mercury in low-rank coal combustion flue gas, Environ. Sci. Technol. 45 (2011) 7394–7400.
[31] L. Xue, C. Zhang, H. He, Y. Teraoka, Catalytic decomposition of N_2O over CeO_2 promoted Co_3O_4 spinel catalyst, Appl. Catal. B 75 (2007) 167–174.
[32] L.F. Liotta, G. Di Carlo, G. Pantaleo, A.M. Venezia, G. Deganello, Co_3O_4/CeO_2 composite oxides for methane emissions abatement: relationship between Co_3O_4–CeO_2 interaction and catalytic activity, Appl. Catal. B 66 (2006) 217–227.
[33] L. Zhao, C. Li, X. Zhang, G. Zeng, J. Zhang, Y. Xie, Oxidation of elemental mercury by modified spent TiO_2-based SCR-DeNO_x catalysts in simulated coal-fired flue gas, Environ. Sci. Pollut. Res. 23 (2016) 1471–1481.
[34] L. Qu, C. Li, G. Zeng, M. Zhang, M. Fu, J. Ma, F. Zhan, D. Luo, Support modification for improving the performance of MnO_x–CeO_y/γ-Al_2O_3 in selective catalytic reduction of NO by NH_3, Chem. Eng. J. 242 (2014) 76–85.
[35] L. Liu, Q. Yu, J. Zhu, H. Wan, K. Sun, B. Liu, H. Zhu, F. Gao, L. Dong, Y. Chen, Effect of MnOx modification on the activity and adsorption of CuO/$Ce_{0.67}Zr_{0.33}O_2$ catalyst for NO reduction, J. Colloid Interface Sci. 349 (2010) 246–255.
[36] I. Atribak, A. Bueno-López, A. García-García, Combined removal of diesel soot particulates and NO x over CeO_2–ZrO_2 mixed oxides, J. Catal. 259 (2008) 123–132.
[37] P. Ning, Z. Song, H. Li, Q. Zhang, X. Liu, J. Zhang, X. Tang, Z. Huang, Selective catalytic reduction of NO with NH3 over CeO_2–ZrO_2–WO_3 catalysts prepared by different methods, Appl. Surf. Sci. 332 (2015) 130–137.
[38] Y. Liu, Y. Wang, H. Wang, Z. Wu, Catalytic oxidation of gas-phase mercury over Co/TiO_2 catalysts prepared by sol–gel method, Catal. Commun. 12 (2011) 1291–1294.
[39] H.S. Roh, W.S. Dong, K.W. Jun, S.E. Park, Partial oxidation of methane over Ni catalysts supported on Ce-ZrO_2 mixed oxide, Chem. Lett. 1 (2001) 88–89.
[40] Z. Ma, X. Wu, Y. Feng, Z. Si, D. Weng, L. Shi, Low-temperature SCR activity and SO_2 deactivation mechanism of Ce-modified V_2O_5–WO_3/TiO_2 catalyst, Prog. Nat. Sci.: Mater. 25 (2015) 342–352.
[41] T. Mondal, K.K. Pant, A.K. Dalai, Catalytic oxidative steam reforming of bio-ethanol for hydrogen production over Rh promoted Ni/CeO_2–ZrO_2 catalyst, Int. J. Hydrogen Energy 40 (2015) 2529–2544.
[42] C.W. Tang, C.B. Wang, S.H. Chien, Characterization of cobalt oxides studied by FT-IR, Raman, TPR and TG-MS, Thermochim. Acta 473 (2008) 68–73.
[43] C.W. Tang, M.C. Kuo, C.J. Lin, C.B. Wang, S.H. Chien, Evaluation of carbon monoxide oxidation over CeO_2/Co_3O_4 catalysts: effect of ceria loading, Catal. Today 131 (2008) 520–525.
[44] K. Asano, C. Ohnishi, S. Iwamoto, Y. Shioya, M. Inoue, Potassium-doped Co_3O_4 catalyst for direct decomposition of N_2O, Appl. Catal. B 78 (2008) 242–249.
[45] S. Youn, S. Jeong, D.H. Kim, Effect of oxidation states of vanadium precursor solution in V_2O_5/TiO_2 catalysts for low temperature NH_3 selective catalytic reduction, Catal. Today 232 (2014) 185–191.
[46] Z. Lian, F. Liu, H. He, Enhanced activity of Ti-modified V_2O_5/CeO_2 catalyst for the selective catalytic reduction of NO_x with NH_3, Ind. Eng. Chem. Res. 53 (2014) 19506–19511.
[47] M.H. Kim, K.H. Choo, Low-temperature continuous wet oxidation of trichloroethylene over CoO_x/TiO_2 catalysts, Catal. Commun. 8 (2007) 462–466.
[48] Z. Song, P. Ning, Q. Zhang, H. Li, J. Zhang, Y. Wang, X. Liu, Z. Huang, Activity and hydrothermal stability of CeO_2–ZrO_2–WO_3 for the selective catalytic reduction of NO_x with NH_3, J. Environ. Sci. 42 (2015) 168–177.
[49] S. Li, Q. Hao, R. Zhao, D. Liu, H. Duan, B. Dou, Highly efficient catalytic removal of ethyl acetate over Ce/Zr promoted copper/ZSM-5 catalysts, Chem. Eng. J. 285 (2016) 536–543.
[50] H. Wang, Z. Qu, H. Xie, N. Maeda, L. Miao, Z. Wang, Insight into the mesoporous $Fe_xCe_{1-x}O_{2-\delta}$ catalysts for selective catalytic reduction of NO with NH_3: regulable structure and activity, J. Catal. 338 (2016) 56–67.
[51] D. Yang, L. Wang, Y. Sun, K. Zhou, Synthesis of one-dimensional $Ce_{1-x}Y_xO_{2-x/2}$ ($0 \le x \le 1$) solid solutions and their catalytic properties: the role of oxygen vacancies, J. Phys. Chem. C 114 (2010) 8926–8932.

[52] B. Shen, Y. Wang, F. Wang, T. Liu, The effect of Ce–Zr on NH_3-SCR activity over MnOx(0.6)/$Ce_{0.5}Zr_{0.5}O_2$ at low temperature, Chem. Eng. J. 236 (2014) 171–180.
[53] F. Bin, C. Song, G. Lv, J. Song, S. Wu, X. Li, Selective catalytic reduction of nitric oxide with ammonia over zirconium-doped copper/ZSM-5 catalysts, Appl. Catal. B 150 (2014) 532–543.
[54] Y. Xu, Q. Zhong, X. Liu, Elemental mercury oxidation and adsorption on magnesite powder modified by Mn at low temperature, J. Hazard. Mater. 283 (2015) 252–259.
[55] W. Shan, F. Liu, H. He, X. Shi, C. Zhang, Novel cerium-tungsten mixed oxide catalyst for the selective catalytic reduction of NO_x with NH_3, Chem. Commun. 47 (2011) 8046–8048.
[56] N.D. Hutson, B.C. Attwood, K.G. Scheckel, XAS and XPS characterization of mercury binding on brominated activated carbon, Environ. Sci. Technol. 41 (2007) 1747–1752.
[57] H. Xu, H. Zhang, S. Zhao, W. Huang, Z. Qu, N. Yan, Elemental mercury (Hg^0) removal over spinel $LiMn_2O_4$ from coal-fired flue gas, Chem. Eng. J. 299 (2016) 142–149.
[58] H. Xu, Z. Qu, C. Zong, W. Huang, F. Quan, N. Yan, MnO_x/graphene for the catalytic oxidation and adsorption of elemental mercury, Environ. Sci. Technol. 49 (2015) 6823–6830.
[59] S.J. Yang, Y.F. Guo, N.Q. Yan, Z. Qu, J.K. Xie, C. Yang, J.P. Jia, Capture of gaseous elemental mercury from flue gas using a magnetic and sulfur poisoning resistant sorbent Mn/gamma-Fe_2O_3 at lower temperatures, J. Hazard. Mater. 186 (2011) 508–515.
[60] S. Tao, C. Li, X. Fan, G. Zeng, P. Lu, X. Zhang, Q. Wen, W. Zhao, D. Luo, C. Fan, Activated coke impregnated with cerium chloride used for elemental mercury removal from simulated flue gas, Chem. Eng. J. 210 (2012) 547–556.
[61] Z. Qu, J. Xie, H. Xu, W. Chen, N. Yan, Regenerable sorbent with a high capacity for elemental mercury removal and recycling from the simulated flue gas at a low temperature, Energy Fuel 29 (2015) 6187–6196.
[62] S. Qiao, J. Chen, J. Li, Z. Qu, P. Liu, N. Yan, J. Jia, Adsorption and catalytic oxidation of gaseous elemental mercury in flue gas over MnO_x/alumina, Ind. Eng. Chem. Res. 48 (2009) 3317–3322.
[63] St G. Christoskovaa, M. Stoyanova, M. Georgieva, D. Mehandjiev, Preparation and characterization of a higher cobalt oxide, Mater. Chem. Phys. 60 (1999) 39–43.
[64] J. Liu, Z. Zhao, J.Q. Wang, C.M. Xu, A.J. Duan, G.Y. Jiang, Q. Yang, The highly active catalysts of nanometric CeO_2-supported cobalt oxides for soot combustion, Appl. Catal. B 84 (2008) 185–195.
[65] D.A. Peña, B.S. Uphade, E.P. Reddy, P.G. Smirniotis, Identification of surface species on titania-supported manganese, chromium, and copper oxide low-temperature SCR catalysts, J. Phys. Chem. B 108 (2004) 9927–9936.
[66] R. Jin, Y. Liu, Z. Wu, H. Wang, T. Gu, Low-temperature selective catalytic reduction of NO with NH_3 over MnCe oxides supported on TiO_2 and Al_2O_3: a comparative study, Chemosphere 78 (2010) 1160–1166.
[67] J.H. Li, J.J. Chen, R. Ke, C.K. Luo, J.M. Hao, Effects of precursors on the surface Mn species and the activities for NO reduction over MnO_x/TiO_2 catalysts, Catal. Commun. 8 (2007) 1896–1900.
[68] S. Ding, F. Liu, X. Shi, H. He, Promotional effect of Nb additive on the activity and hydrothermal stability for the selective catalytic reduction of NO_x with NH_3 over $CeZrO_x$ catalyst, Appl. Catal. B 180 (2016) 766–774.
[69] J. Wang, Z. Yan, L. Liu, Y. Chen, Z. Zhang, X. Wang, In situ DRIFTS investigation on the SCR of NO with NH_3 over V_2O_5 catalyst supported by activated semi-coke, Appl. Surf. Sci. 313 (2014) 660–669.
[70] D. Sun, Q. Liu, Z. Liu, G. Gui, Z. Huang, Adsorption and oxidation of NH_3 over V_2O_5/AC surface, Appl. Catal. B 92 (2009) 462–467.
[71] W. Shan, F. Liu, H. He, X. Shi, C. Zhang, A superior Ce-W-Ti mixed oxide catalyst for the selective catalytic reduction of NO_x with NH_3, Appl. Catal. B 115 (2012) 100–106.
[72] G. Qi, R.T. Yang, R. Chang, MnO_x-CeO_2 mixed oxides prepared by co-precipitation for selective catalytic reduction of NO with NH_3 at low temperatures, Appl. Catal. B 51 (2004) 93–106.
[73] M. Kantcheva, A.S. Vakkasoglu, Cobalt supported on zirconia and sulfated zirconia I.: FT-IR spectroscopic characterization of the NO_x species formed upon NO adsorption and NO/O_2 coadsorption, J. Catal. 223 (2004) 352–363.
[74] K. Hadjiivanov, H. Knözinger, Species formed after NO adsorption and NO + O_2 co-adsorption on TiO_2: an FTIR spectroscopic study, Phys. Chem. Chem. Phys. 2 (2000) 2803–2806.
[75] X. Zhang, H. He, H. Gao, Y. Yu, Experimental and theoretical studies of surface nitrate species on Ag/Al_2O_3 using DRIFTS and DFT, Spectrochim. Acta Part A 71 (2008) 1446–1451.
[76] Y. Shu, H. Sun, X. Quan, S. Chen, Enhancement of catalytic activity over the iron-modified Ce/TiO_2 catalyst for selective catalytic reduction of NO_x with ammonia, J. Phys. Chem. C 116 (2012) 25319–25327.
[77] Z. Liu, Y. Liu, Y. Li, H. Su, L. Ma, WO3 promoted Mn–Zr mixed oxide catalyst for the selective catalytic reduction of NO_x with NH_3, Chem. Eng. J. 283 (2016) 1044–1050.
[78] P.R. Ettireddy, N. Ettireddy, T. Boningari, R. Pardemann, P.G. Smirniotis, Investigation of the selective catalytic reduction of nitric oxide with ammonia over Mn/TiO_2 catalysts through transient isotopic labeling and in situ FT-IR studies, J. Catal. 292 (2012) 53–63.